EFFECTIVE SHUNT IMPEDANCE COMPARISON BETWEEN S-BAND STANDING WAVE ACCELERATORS WITH ON-AXIS AND OFF-AXIS COUPLERS

S.O. Schriber, L.W. Funk and R.M. Hutcheon
Atomic Energy of Canada Limited
Physics Division, Chalk River Nuclear Laboratories
Chalk River, Ontario, Canada K0J 1J0

Summary

The effective shunt impedances of a side-coupled S-band standing wave accelerating structure and a structure employing on-axis couplers have been compared by measuring the energy of accelerated electrons. The structures had similar cell grading, were assembled using similar techniques and operated in the $\pi/2$ mode. The energy of the accelerated electrons was measured with a calibrated 30° analyzing magnet. Two on-axis coupled structures both had a 10% higher effective shunt impedance than the side-coupled structure; their shunt impedances were $\sim$ 95% of the theoretical value.

Criteria for choosing an on-axis coupled structure compared to side-coupled and "disc and washer" accelerating structures are given.

Introduction

The requirement for proton accelerators capable of accelerating beams to energies in excess of 200 MeV for meson or neutron factories[1,2] has stimulated considerable development in linear accelerator design. The dominant objective of this development has been to reduce costs through higher rf efficiency and simpler tuning and assembly.

The cost of the rf power supply is a major contributor to the total cost of a large proton linac. Any increase in accelerating structure shunt impedance reduces this cost. Improvements in shunt impedance gained by shaping[3] the cavities of standing wave accelerators are well known. The side-coupled $\pi/2$ mode accelerating structure design[4] used for the high energy portion of LAMPF[1] is an example.

Simplified tuning and assembly also reduce costs. The disc-and-washer loaded structure proposed by Andreev et al.[5] was designed to have these advantages. It has stronger intercavity coupling and a shunt impedance almost as high as the side-coupled design.

This paper compares the design and measured shunt impedance of a side-coupled accelerating structure with that of two nearly identical standing wave accelerating structures with on-axis couplers[4]. Because the on-axis coupling cavities provide no accelerating field, the effective shunt impedance, ZT^2, of the on-axis coupled systems was expected to be less than that of an equivalent side-coupled structure. Instead, the on-axis coupled structures had a 10% higher effective shunt impedance, higher than previously reported[6].

An on-axis coupled structure combines a high shunt impedance with the simpler tuning and assembly of the disc-and-washer loaded structure. In addition, second neighbour coupling between accelerating cavities can be eliminated and intercavity coupling of non-axially symmetric modes such as the TM_{110}-like beam break-up mode can be minimized. Both coupling effects were minimized by orienting successive pairs of coupling slots in the cavity walls 90° to each other. The advantages of an on-axis coupled standing wave structure make it preferable both for the high energy portion of a proton linac and for electron linacs.

Accelerating Structure Description

Theory

The profile of the 3 GHz accelerating cavities shown in Figure 1 is similar to that used by the graded-beta 0.8 GHz accelerating structure discussed by McKeown et al.[7]. This $\beta = 0.65$ profile was chosen because individual cavity frequencies are independent of cavity length. Different cavity lengths from $\beta = 0.6$ to $\beta = 1.0$ are obtained by subtracting or adding a right circular cylindrical section to the basic $\beta = 0.65$ length. The calculated decrease in ZT^2 from cavities with fully optimized profiles, is less than 1%; thus identical profiles can be used for the $\beta > 0.6$ structures of a long proton linac at a negligible penalty.

The effective shunt impedance of a group of identical cavities (profiles shown in Figure 1) operating in the π mode was calculated by a numerical mesh computer program[8] similar to LALA[3]. The π mode simulated the $\pi/2$ mode field distribution in a coupled cavity structure because there are no fields in the coupling cavities. A polynomial least squares fit to these calculated values as a function of cavity length gave the following relationship.

$$ZT^2(M\Omega/m) = \frac{2Af^{1/2}}{\beta}\,(28.26 + 105.54\,A - 93.76\,A^2)$$

$$\text{where } A = \beta/2 + (0.00766/f - 2t_w)/\lambda,\ L = \beta\lambda/2,$$

f is the rf resonant frequency in GHz, L is the length of the cavity in m, t_w is the effective web thickness as shown in Figure 1 in m and λ is the rf wavelength in m. The 3 GHz side-coupled structure had a web thickness of 3.17 mm to support the drift tube noses rigidly. The on-axis coupled structure had an effective web thickness of 3.96 mm comprised of a 1.57 mm space for one half of the on-axis coupling cavity and a 2.39 mm web thickness for rigidly supporting the drift tube nose. The 3.14 mm length of the on-axis coupling cavity was a reasonable compromise between being too long (reducing the structure ZT^2) and being too short (leading to

multipactoring, arcing and reduced coupling). There has been no evidence of multipactoring or arcing in these S-band on-axis coupling cavities for accelerating gradients from 1 MeV/m to 18 MeV/m[6]. Figure 2 gives a comparison of the calculated ZT^2 for the two types of accelerating structures from $\beta = 0.6$ to $\beta = 1.0$, illustrating the theoretical advantage of the side-coupled structure.

Design and Fabrication

The two types of structures shown in Figure 3 were tested in the $\pi/2$ mode at 3 GHz. The on-axis coupled structures were 1.6 m in length and each consisted of 33 accelerating cavities and 32 coupling cavities. The 1 m long side-coupled structure similar to that described by McKeown et al.[7] consisted of 21 accelerating cavities and 20 coupling cavities. All structures were designed to operate with an average accelerating gradient of 8 MeV/m and the first four cavities were graded in beta to accept 40 keV electrons from an electron gun. Rf power was coupled to the structure via an oval iris in the central accelerating cavity. The interface between the accelerator vacuum and the pressurized waveguide was a thin Al_2O_3 window. Capacitive rf probes monitored average electric fields in the first, central and last cavities.

For each accelerating structure the individual cavity frequencies were tuned within ± 500 kHz of the average and the passband gap was made less than 500 kHz. These tolerances ensured that axial rf electric field amplitudes in the coupling cavities would be less than 5% of those in the accelerating cavities, as verified by bead pull measurements on the on-axis coupled structure. The coupling constant was made 5% to ensure that adjacent modes would contribute less than 1% of the $\pi/2$ mode rf field. Individual coupling constants were made equal to within 1% to ensure that rf fields in adjacent accelerating cavities would be equal to within 1% and to ensure that any systematic rf field difference along the structure would not exceed 10%. Bead pull measurements on both types of structures verified that in fact the field differences were < 5%, sufficiently small to introduce negligible errors in the ZT^2 measurements.

Brazing techniques for the two types of structures differed because the side-coupled system required more brazing steps. For the side-coupled structure 50Au-50Cu braze alloy was used to fabricate side-couplers from component halves and for the segment to segment braze. Side-couplers on one side were joined to the brazed segment assembly using 50Au-50Cu alloy while 72Ag-28Cu alloy was used to braze the remaining side-couplers to the opposite side of the segment assembly. Components for the on-axis coupled structure were brazed[9] using 72Ag-28Cu alloy except for one joint in the iris coupling cavity and two stainless steel end flanges which were brazed using 68Ag-27Cu-5Pd alloy. All structures were cleaned prior to and after brazing using the same techniques. After assembly of the complete vacuum envelope, the accelerator system shown in the upper part of Figure 4 was baked at 120°C for several days - the temperature being limited by some of the diagnostic components.

Apparatus

A block diagram of the apparatus is shown in Figure 4. The 2 MW, 0.1% duty factor rf power source was a tuneable M-5125 English Electric magnetron. The rf waveguide included a 23 db Raytheon circulator for isolation, a phase shifter to optimize magnetron-resonant load frequency lock, directional couplers to monitor forward and reverse power at two locations and a waveguide switch to direct rf either to the accelerating structure or to a water load. The waveguide was pressurized with SF_6 to 375 kPa to prevent breakdown at the circulator. Average rf power was measured calorimetrically using a dummy water load (VSWR < 1.03) with a good thermal response time. The calorimetric system, which used a calibrated turbine flowmeter to measure flowrates and a thermopile to measure temperature rise, was calibrated in situ with a dc powered immersion heater before and after each set of electron beam measurements at a particular power level.

The diode electron guns were driven at 40 kV by the magnetron HV pulse. The accelerators with on-axis couplers used a gun approximating Pierce geometry with 0.25 mm diameter thoriated tungsten wire wound to form a 15.2 mm inside diameter annular cathode. The side-coupled accelerator described earlier[10] used a Pierce geometry gun with a 3 mm diameter dispenser cathode.

Focussing and steering elements at the entrance and exit of the structures were used to offset effects of space charge forces, rf defocussing and misalignment.

A 30° magnet with a radially focussed, momentum dispersed image at an 0.5 mm slit, 0.18 m from the magnet, analyzed the electron beam. The magnet was excited by a current regulated power supply and its gap field was measured using a calibrated Hall probe. The relationship between electron beam energy and magnetic field was obtained using the electron beam transport computer code TRANSPORT[11] and was verified by numerical beam trajectory computer calculations using mapped fields of the 30° magnet.

The beam current transmitted through the analyzer slits was collected in a Faraday cup. With the analyzing magnet off, a second Faraday cup coaxial with the accelerator axis measured the total accelerated electron beam and ensured that the output beam was properly aligned. Current monitoring toroids at the accelerator entrance and exit gave additional beam current information for determining accelerator stability.

Pressures of less than 10^{-4} Pa with rf and beam on were maintained by noble-gas ion pumps which were attached to the electron gun, the major gas load of each system.

Method

Current pulses from the Faraday cup measuring the analyzed beam were fed into a sample and hold unit which sampled the central 2 μs of the 3 μs beam pulse and produced a dc signal for display on the y axis of an x-y recorder; the x-axis recorded the

analyzing magnet coil current. The voltage-controlled, current-regulated magnet power supply was driven by a saw tooth voltage ramp. Periodic magnetic field to coil current calibration checks were made with the Hall probe.

A spectral measurement took approximately 20 seconds, during which the magnetron voltage and current, forward and reverse rf power, accelerating field and beam current were monitored to make sure conditions were sufficiently stable. Repeated measurements were also used to check stability. An automatic frequency control system kept the magnetron locked to the accelerators to within 40 kHz.

Peak rf power was determined from the average rf power using the pulse repetition rate and the rf pulse shape. Average power was measured using the water load, and the pulse shape was measured using a crystal detector mounted on the forward port of the directional coupler adjacent to the waveguide switch. Peak power corrections were made to account for reflected power using the $\pi/2$ mode structure VSWR determined from low power (0.1 watt) rf measurements. The largest correction was 6.3% for one of the on-axis coupled structures which had an overcoupled VSWR of 1.67.

The effective shunt impedance was calculated from

$$ZT^2(M\Omega/m) = \frac{(E_{MAX} - E_{INJ})^2}{(P - I\,E_{MEAN})L}$$

where P is the peak rf power in MW corrected for reflections from the accelerating structures, L is the length of the accelerating structure in m, I is the accelerated beam current in A and E_{INJ}, E_{MEAN} and E_{MAX} are the injected, mean accelerated and maximum accelerated beam energy in MeV, respectively.

Thirteen independent ZT^2 measurements for one of the on-axis coupled structures had an average value of 82.0 ± 0.8 MΩ/m. The quoted uncertainty results from a quadrature addition of the standard deviation error of the series of measurements and the errors associated with the estimated uncertainties in each measured variable. Conditions for each measurement were quite different as the peak rf power from the magnetron ranged from 0.8 to 1.8 MW and the peak accelerated current, from 0.04 mA to 5 mA.

Another method for determining ZT^2 is shown in Figure 5 where the maximum beam energy is plotted as a function of accelerated beam current for constant peak rf power. During a series of measurements at one power level, only the injected current from the electron gun was varied by changing cathode emission. A straight line was least squares fitted to the results and the shunt impedance was determined from its slope using an expression based on a summation of beam and structure powers.

$$E_{MAX} = (ZT^2 PL)^{1/2} - (ZT^2\,L/2)I$$

For these experiments this equation is accurate to within 2% for I less than 40 mA. The average ZT^2 from the results shown in Figure 5 was 82 ± 2 MΩ/m. Combining all the results, the measured ZT^2 for the on-axis coupled structure was 82.0 ± 0.9 MΩ/m. Similar measurements on the second on-axis coupled structure yielded a ZT^2 of 83 ± 2 MΩ/m. The theoretical ZT^2 for these structures including the effect of the graded-beta section was 86.5 MΩ/m.

Measurements on the side-coupled structure using the same techniques and the same measuring equipment described above gave a ZT^2 of 73 ± 2 MΩ/m, 80% of the theoretical 90.7 MΩ/m for this structure. This 20% difference agrees with measurements[7,12] on 0.8 GHz side-coupled accelerating structures and has been attributed to the coupling slots and copper surface finish.

Discussion

The measured ZT^2 for the on-axis coupled structure, close to $\beta = 1$, was 10% higher than for a similar side-coupled structure, although it was expected to be 5% less because of the space occupied by the coupling cavities on the beam accelerating axis. Scaling the results of the measurements to 0.8 GHz cavities with profiles similar to Figure 1 gave the results shown in Figure 6 for the practical effective shunt impedance as a function of β for a side-coupled accelerating structure with t_w = 4.76 mm (the LAMPF value[3]) and an on-axis coupled accelerating structure with t_w = 10.61 mm (4.76 mm web thickness and 5.85 mm on-axis coupled cavity scaled from the S-band value). These results show that, compared to a side-coupled structure, the on-axis coupled structure has a 10% higher ZT^2 at $\beta = 1$ and a 3% higher ZT^2 at $\beta = 0.6$.

For a particular application the necessary web thickness of an on-axis coupled structure will usually be different from that of a side-coupled structure because of cooling, mechanical strength and rf coupling requirements. Since ZT^2 depends on web thickness it is clear that the structure chosen for maximum shunt impedance will depend on the application.

Figure 6 also shows the expected ZT^2 for a 0.8 GHz disc-and-washer loaded accelerating structure using the calculated values of Andreev et al.[5] and their minimum estimate of a 5% loss in ZT^2 for a practical cavity. The on-axis coupled structure has a 20% to 10% higher effective shunt impedance than an equivalent disc-and-washer structure from $\beta = 0.6$ to $\beta = 1.0$, respectively.

Conclusions

On-axis coupled accelerating structures have been found to have an effective shunt impedance higher than an equivalent side-coupled structure, or a disc-and-washer loaded structure for $\beta > 0.6$. Achievement of 95% of the theoretical shunt impedance cannot be explained by acceleration from coupling cavity fields because they were less than

5% of the accelerating cavity fields. Different braze alloy was used for brazing segments of the two types of structures. The difference in ZT^2 between the side-coupled and on-axis coupled structures cannot be explained by alloy conductivity differences because there was no appreciable amount of alloy on the inner conducting surfaces. Any unaccounted systematic error in the measurements would not change the comparative results between the side-coupled and on-axis coupled structures since the measurements employed the same instruments and techniques. In any case the difference between the S-band side-coupled measurement and theory is in agreement with results on 0.8 GHz structures[7,12].

The on-axis coupled structure has several advantages over an equivalent side-coupled structure. Machining is not difficult and tuning and assembly techniques[9] have been determined which are simpler because the on-axis coupled structure consists of coaxial components.

Second neighbour coupling between adjacent accelerating cavities is eliminated by orienting successive pairs of coupling slots 90° to each other. There can be no rf currents on connecting walls between adjacent accerating cavities as with a side-coupled structure which has a second neighbour coupling $\sim$ 1/10 of first neighbour coupling; this may partially explain the higher ratio of measured to theoretical shunt impedance for an on-axis coupled structure.

Another advantage of this coupling arrangement is that propagation of non-axially symmetric modes such as the TM_{110}-like mode is minimized. Larger beam currents could be accelerated by an on-axis coupled structure than by present side-coupled structures because beam break-up current limits are higher. However orienting alternate side-couplers by 90° rather than the usual 180° would achieve the same result in a side-coupled structure. The on-axis coupled structure has the same advantage over the disc-and-washer structure which may have coupling for the TM_{110}-like modes as strong as or higher than that for the desired TM_{010}-like accelerating mode.

The disc-and-washer structure has an inter-cavity coupling constant about ten times that of a side-coupled or an on-axis coupled system. This should result in looser assembly tolerances related to cavity frequency differences. However, relative cavity field levels are still associated with relative inter-cavity coupling constant differences and it has been noted[4,13] that this effect puts a stringent requirement on these tolerances; consequently the disc-and-washer structure has the same tolerance as the side-coupled or on-axis coupled structure for individual cavity coupling constants.

Larger coupling constants imply that longer chains of cavities can be coupled before effects from adjacent modes or high beam loading begin to alter the $\pi/2$ mode relative rf field levels along the cavity chain. Calculations have shown that a single 4 m S-band structure (70 accelerating cavities) with on-axis couplers and 5% inter-cavity coupling could be assembled with modes adjacent to the $\pi/2$ mode contributing to less than 2% of the $\pi/2$ rf fields if the drive is at the central cavity. Using the same criterion, the disc-and-washer structure could be ten times the length of an on-axis coupled structure. However, brazing furnace length and rf tube size limitations may reduce the importance of this advantage. Beam break-up effects associated with TM_{110}-like modes may reduce the capability of the disc-and-washer system to handle very high beam loading.

The on-axis coupled structure is easily cooled by symmetrically located channels which cover the length of the structure at its circumference. There is no need to provide separate cooling for the couplers as was required for 0.8 GHz side-coupled accelerating structures. No water-vacuum joints where leaks cannot be located and repaired are necessary as are required for the disc-and-washer structure.

The on-axis coupled accelerating structure is an attractive choice for linear accelerators which are accelerating particles with $\beta > 0.6$ because it has a high effective shunt impedance, it reduces beam break-up effects associated with the TM_{110}-like mode, it is easy to cool symmetrically and it has simple assembly procedures which should result in cost savings. The disc-and-washer structure may be preferred in situations which require very long single accelerating structures.

Acknowledgements

The authors would like to thank L.D. Molson who assisted with the calibration of the 30° analyzing magnet and K.J. Hohban who participated in obtaining the experimental results.

References

1. D.E. Nagle, Proc. of 1964 Linac Conf., MURA-714, 94 (1964).

2. G.A. Bartholomew and P.R. Tunnicliffe, eds., Atomic Energy of Canada Limited, Report AECL-2600 (1966).

3. H.C. Hoyt, D.D. Simmons and W.F. Rich, Rev. Sci. Instr. 37, 755 (1966).

4. E.A. Knapp, B.C. Knapp and J.M. Potter, Rev. Sci. Instr. 39, 979 (1968).

5. V.G. Andreev, V.M. Belugin, V.G. Kulman, E.A. Mirochnik and B.M. Pirozhenko, Proc. of 1972 Proton Linac Conf., LA-5115, 114 (1972).

6. S.O. Schriber, E.A. Heighway and L.W. Funk, Proc. of 1972 Proton Linac Conf., LA-5115, 140 (1972).

7. J. McKeown, H.R. Schneider and S.O. Schriber, Proc. of 1972 Proton Linac Conf., LA-5115, 233 (1972).

8. O. Aboul-Atta and A. Malecki, CRNL, private communication.

9. S.B. Hodge, L.W. Funk and S.O. Schriber, Proc. of this conference.

10. S.O. Schriber and E.A. Heighway, IEEE Trans. Nucl. Sci., NS-22, No. 3, 1060 (1975).

11. K.L. Brown and S.K. Howry, SLAC-91 (1970).

12. E.A. Knapp, P.W. Allison, C.R. Emigh, L.N. Engel, J.M. Potter and W.J. Shlaer, Proc. of 1966 Linac Conf., LA-3069, 83 (1966).

13. S.O. Schriber, IEEE Trans. Nucl. Sci., NS-22, No. 3, 1343 (1975).

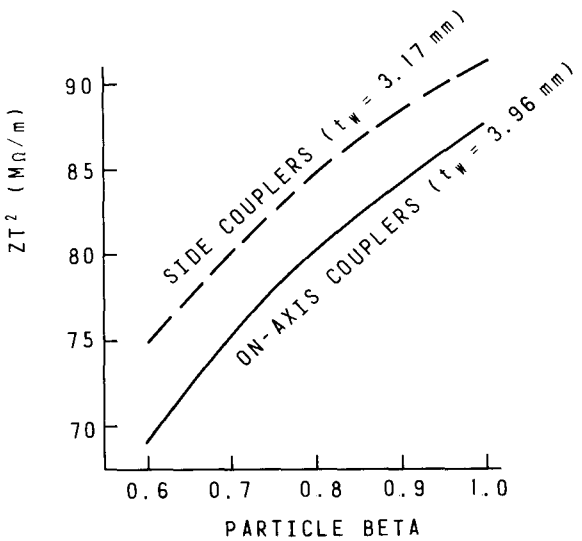

Fig. 2. Calculated ZT^2 as a function of particle beta for 3 GHz accelerating structures. Cavity length, L, is given by $\beta\lambda/2$.

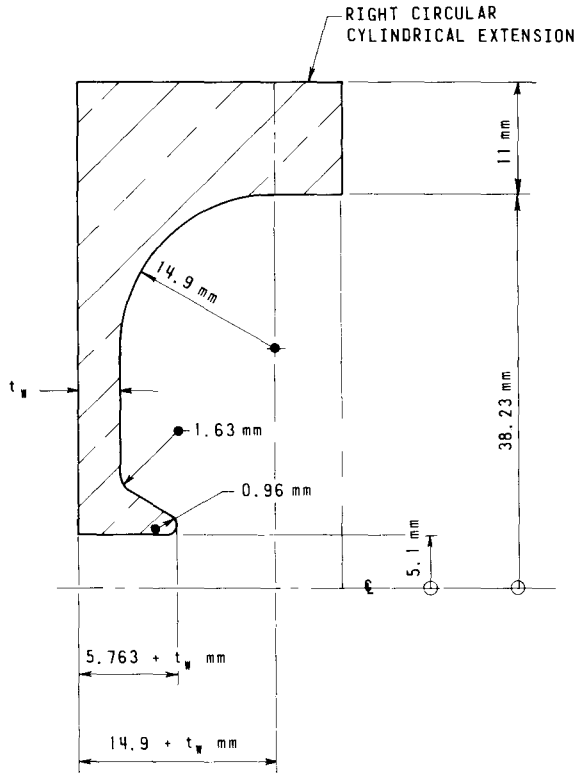

Fig. 1. 3 GHz cavity profile based on $\beta = 0.65$ shape plus right circular cylinder extension.

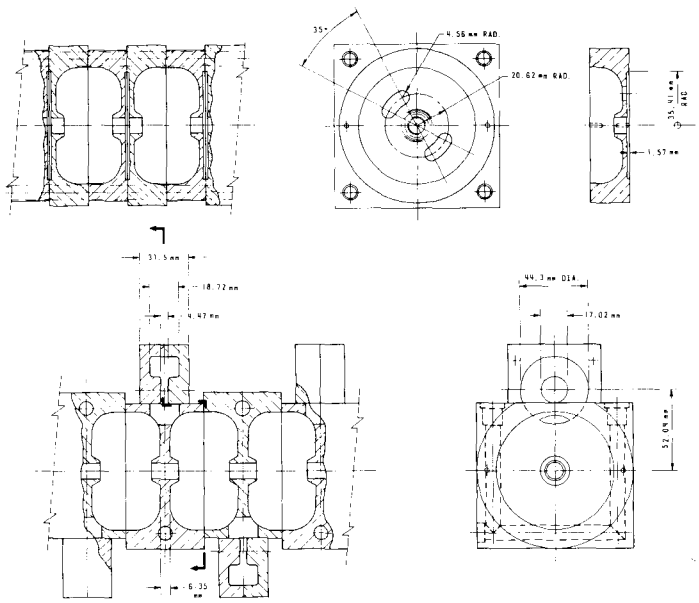

Fig. 3. Cutaway view of the on-axis coupled (a) and side-coupled (b) accelerating structures.

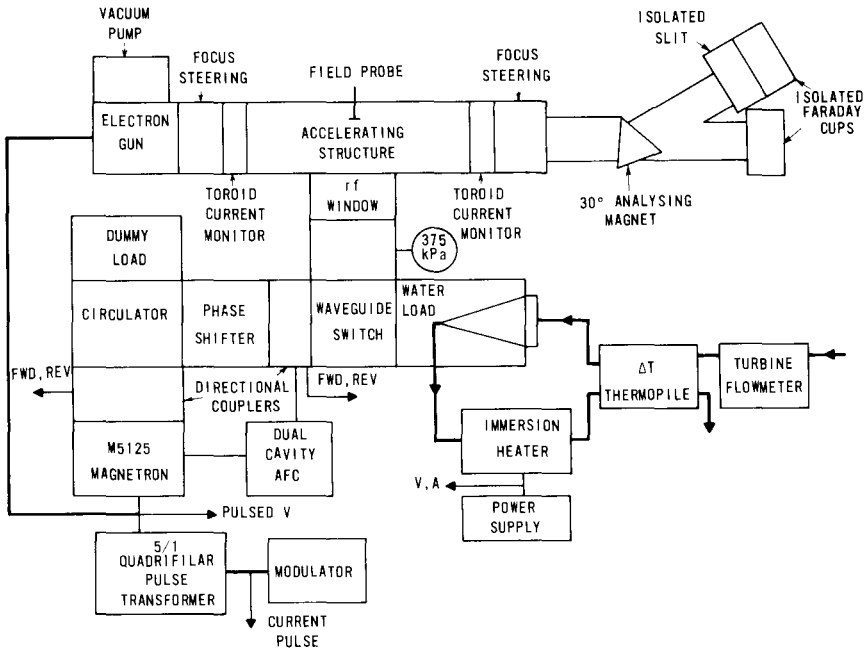

Fig. 4. Schematic layout of accelerator, rf power system and monitoring components.

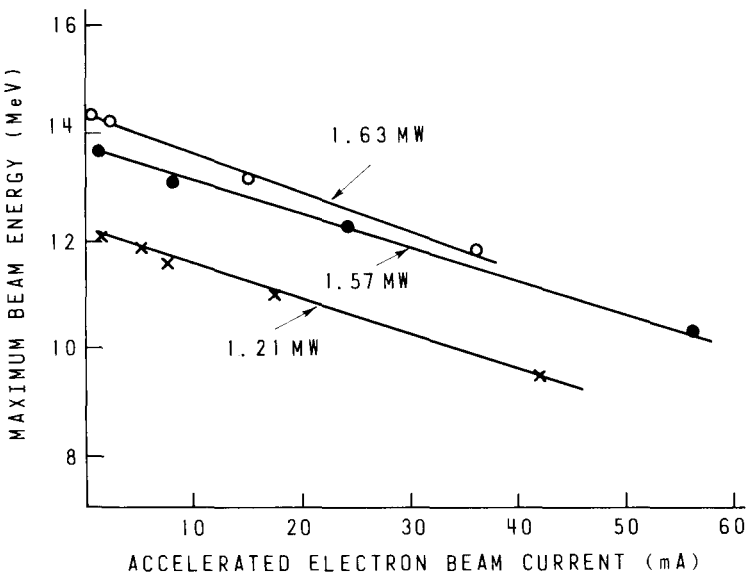

Fig. 5. Maximum beam energy from the 1.6 m on-axis coupled structure as a function of the accelerated beam current for different peak rf power output from the magnetron.

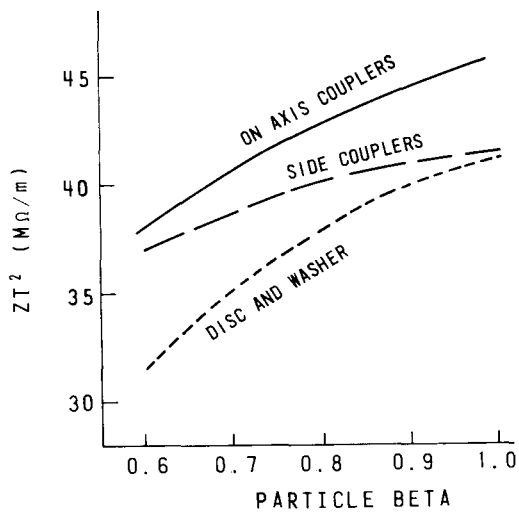

Fig. 6. Expected ZT^2 as a function of particle beta for 0.8 GHz accelerating structures. Cavity length, L, is given by $\beta\lambda/2$.